Cross-Correlated Relaxation of Dipolar Coupling and Chemical-Shift Anisotropy in Magic-Angle Spinning R 1ρ NMR Measurements: Application to Protein Backbone Dynamics Measurements

Vilius Kurauskas, Emmanuelle Weber, Audrey Hessel, Isabel Ayala, Dominique Marion, Paul Schanda

▶ **To cite this version:**

Vilius Kurauskas, Emmanuelle Weber, Audrey Hessel, Isabel Ayala, Dominique Marion, et al.. Cross-Correlated Relaxation of Dipolar Coupling and Chemical-Shift Anisotropy in Magic-Angle Spinning R 1ρ NMR Measurements: Application to Protein Backbone Dynamics Measurements. Journal of Physical Chemistry B, 2016, 120 (34), pp.8905-8913. 10.1021/acs.jpcb.6b06129 . hal-01382208

HAL Id: hal-01382208
https://hal.science/hal-01382208

Submitted on 18 Oct 2016

HAL is a multi-disciplinary open access archive for the deposit and dissemination of scientific research documents, whether they are published or not. The documents may come from teaching and research institutions in France or abroad, or from public or private research centers.

L'archive ouverte pluridisciplinaire **HAL**, est destinée au dépôt et à la diffusion de documents scientifiques de niveau recherche, publiés ou non, émanant des établissements d'enseignement et de recherche français ou étrangers, des laboratoires publics ou privés.

Cross-Correlated Relaxation of Dipolar Coupling and Chemical-Shift Anisotropy in Magic-Angle Spinning $R_{1\rho}$ NMR Measurements: Application to Protein Backbone Dynamics Measurements

Vilius Kurauskas[1,2,3], Emmanuelle Weber[1,2,3], Audrey Hessel[1,2,3], Isabel Ayala[1,2,3], Dominique Marion[1,2,3,*] and Paul Schanda[1,2,3,*]

1 CEA, Institut de Biologie Structurale (IBS), 38027 Grenoble, France

2 CNRS, Institut de Biologie Structurale (IBS), 38027 Grenoble, France

3 Université Grenoble Alpes, IBS, 38027 Grenoble, France

Author Information

Corresponding authors:

* Address: Institut de Biologie Structurale, 71 avenue des martyrs, F-38044 Grenoble Cedex, France. E-mail: dominique.marion@ibs.fr and paul.schanda@ibs.fr

Keywords: protein, rotating frame relaxation, numerical spin simulations, spin-diffusion, J-doublet.

Abstract

Transverse relaxation rate measurements in MAS solid-state NMR provide information about molecular motions occurring on nanoseconds-to-milliseconds (ns-ms) time scales. The measurement of heteronuclear (^{13}C, ^{15}N) relaxation rate constants in the presence of a spin-lock radio-frequency field ($R_{1\rho}$ relaxation) provides access to such motions, and an increasing number of studies involving $R_{1\rho}$ relaxation in proteins has been reported. However, two factors that influence the observed relaxation rate constants have so far been neglected, namely (i) the role of CSA/dipolar cross-correlated relaxation (CCR), and (ii) the impact of fast proton spin flips (i.e. proton spin diffusion and relaxation). We show that CSA/D CCR in $R_{1\rho}$ experiments is measurable, and that this cross-correlated relaxation rate constant depends on ns-ms motions, and can thus itself provide insight into dynamics. We find that proton spin-diffusion attenuates this cross-correlated relaxation, due to its decoupling effect on the doublet components. For measurements of dynamics, the use of $R_{1\rho}$ rate constants has practical advantages over the use of CCR rates, and the present manuscript reveals factors that have so far been disregarded and which are important for accurate measurements and interpretation.

Introduction

The structure of a protein is determined by a large number of individually weak interactions, which constantly re-shuffle at ambient temperatures. This dynamic exchange between different conformers is often important for functions such as binding or enzymatic turnover. NMR spectroscopy is very well suited to provide direct atomic-level access to the amplitudes and time scales of such motions. Whereas solution-state NMR is a well-established tool for such studies, magic-angle spinning (MAS) solid-state NMR (ssNMR) is rapidly establishing in studies of biomolecular dynamics, complementing its solution-state counterpart in cases where limited solubility or large size hamper the application of solution-state methods. In addition to opening new fields of applications, ssNMR also has theoretical advantages for determining dynamics, compared to solution-state NMR. In particular, the absence of overall tumbling motion enables the study of motions without "blind windows" of time scales, i.e. over all time scales from picoseconds to seconds, in contrast to its solution-state counterpart, which is severely challenged on the nanosecond to several-microseconds time scale.[1] In MAS ssNMR, motions can be studied through (i) their averaging effect on anisotropic interactions (in particular, the averaging of dipolar couplings and chemical-shift anisotropies), which report on the amplitude of motion seen by these interactions, and (ii) through the investigation of nuclear spin relaxation rate constants, which depend on amplitudes and time scales of motions. Many biological processes, such as binding, gating or enzymatic turnover, occur on time scales of hundreds of nanoseconds to milliseconds (ns-ms). Studying these time scales is, therefore, of particular relevance when attempting to decipher the molecular basis of these processes. In MAS ssNMR, motion on these time scales can be accessed by measurements of transverse relaxation rate constants, such as the decay of spin coherence, R_2. However, quantitative measurements of transverse relaxation rates in ssNMR are generally hampered by the fact that spin coherences in solid samples decay through two mechanisms, (i) due to random field fluctuations (i.e., dynamics), which is what we are interested in herein, and (ii) due to evolution under the incompletely averaged anisotropic interactions, in particular due to ^{1}H-^{1}H dipolar couplings. The latter, termed dipolar dephasing, strongly depends on the presence of (multiple) dipolar couplings, and on the employed MAS frequency. Accessing the dynamics-induced component requires that coherent contributions to signal decay (in particular dipolar dephasing) are suppressed to negligible levels. Several reported studies have shown that heteronuclear (^{13}C, ^{15}N) $R_{1\rho}$ rate constants, i.e. the decay of C_x (N_x) in the presence of a spin-lock RF field, can be measured accurately without significant interfering effects from dipolar dephasing if (i) high MAS frequencies and/or (ii) extensive deuteration are applied.[2–5] $R_{1\rho}$ experiments under such conditions have been reported so far for ^{15}N and ^{13}C' sites in small model proteins (SH3, GB1, ubiquitin).[2–7] $R_{1\rho}$ experiments in solids are particularly informative also when the RF field strength approaches the rotary resonance conditions, as has been shown for small molecules[8,9] and proteins.[4,6]

As an alternative method to probe ns-ms motions, it has been proposed to measure cross-correlated relaxation (CCR) between ^{1}H-^{15}N dipolar/^{15}N chemical-shift anisotropy (CSA) interactions in R_2'-type experiments (i.e. in the absence of a spin-lock RF field). These latter experiments measure the difference of the apparent transverse decay rate constants of the two ^{15}N scalar-coupling doublet

components, i.e. the decay of N_x-[H^α] and N_x-[H^β] components in a spin-echo experiment.[10] Even though each individual rate constant itself contains contributions from dipolar dephasing (and can, therefore, not be interpreted quantitatively), the respective difference can be quantitatively interpreted in terms of dynamics on ns-ms time scales.[11] This experiment suffers, however, from the fact that the R_2' decay rates in MAS ssNMR are large, because of the dipolar-dephasing contribution. As a consequence, detection of a small differential relaxation rate from two individually large relaxation rate constants corresponding to the two doublet components (R_2'+$\Gamma^{CSA/D}$ and R_2'-$\Gamma^{CSA/D}$) is challenging. Furthermore, the rapid signal loss throughout the experiment, based on scalar-coupling transfers,[10] results in relatively low detection sensitivity.

Here we investigate the effects of dipolar/CSA CCR in heteronuclear (^{13}C, ^{15}N) $R_{1\rho}$ experiments in MAS ssNMR. In solution-state NMR, such cross-correlated relaxation effects have been reported[12,13], but have so far been neglected in MAS ssNMR. We use explicit numerical spin dynamics simulations, as well as experimental measurements, and show that CCR rate constants under spin-lock RF fields are measurable, and that they report on molecular motion. The CCR rate constant has a similar dependence on dynamics as the in-phase $R_{1\rho}$ rate constant, as we show with numerical simulations. We assume here that the CCR rate constant in $R_{1\rho}$ measurements is essentially free from coherent contributions, for several reasons. First, it has been convincingly shown that CCR rate constants, derived from the above-mentioned experiments with free evolution (R_2') are primarily reflecting dynamics, even though each of the two doublet components itself is not free from coherent contributions.[14] In $R_{1\rho}$- based experiments the situation can be assumed to be even more favorable, because the decay of each of the two components is much less prone to coherent decay.[3]

Furthermore, we show that experimentally determined $R_{1\rho}$-derived CCR rate constants (referred to here as $\Gamma_{1\rho}^{CSA/D}$) reveal the expected patterns of motions in a well-studied protein, and correlate with $R_{1\rho}$ rate constants, which have been shown to contain only minimal coherent contributions. However, both CCR and $R_{1\rho}$ contain contributions from stochastic proton flips: we provide evidence that proton spin-diffusion reduces the CCR rate constants due to averaging of the doublet components. Furthermore, proton spin diffusion also leads to an increase of the auto-relaxation ($R_{1\rho}$) rate constants, in a manner that depends on the RF field strength. Our experimental data and simulations thus suggest that knowledge of the proton spin-diffusion rate is required for accurately determining dynamics, either through in-phase $R_{1\rho}$ measurements or CCR measurements under spin-lock. Finally, we also discuss pulse schemes to suppress the effects of CCR, and thus eliminate the bi-exponentiality of decay in in-phase $R_{1\rho}$ measurements.

Materials and Methods

Samples and NMR spectroscopy

In this study we investigate the cross-correlated relaxation between a heteronuclear CSA tensor (^{15}N) and the ^{1}H-^{15}N dipolar coupling in amide moieties; our conclusion apply also to other ^{1}H-X spin pairs, such as ^{1}H-^{13}C in backbone or side chain sites. We use u-[^{2}H,^{15}H]-labelled ubiquitin, crystallized with 2-methyl-2,4-pentane-diol (MPD)[15], obtained by crystallization from a solution containing an effective H_2O/D_2O ratio of 60/40 (taking into account protons originating from MPD). Exchangeable sites, such as amides are protonated at a level of 60%, in an otherwise deuterated background. Protein samples were filled into 1.6 mm Agilent MAS rotors by ultracentrifugation using a dedicated filling device (in-house built). NMR experiments were performed on a 600 MHz Agilent VNMRS spectrometer equipped with a 1.6 mm MAS probe tuned to ^{1}H,^{13}C,^{15}N frequencies, spinning at 38 kHz MAS frequency. The effective sample temperature, calibrated with internal standard using the bulk water frequency, was set to 300 K. Pulse sequences used in this study are shown in Figure S1 in the Supporting Information, and use ^{1}H-^{15}N out-and-back cross-polarization, and ^{1}H detection. In particular, the sequence in Figure S1B was used for the CCR measurement, and (in-phase) $R_{1\rho}$ rate constants with and without ^{1}H π pulse decoupling are shown in Figure S1A and C, respectively. Finally, the proton spin-diffusion experiment was performed with the sequence shown in Figure S1D. ^{15}N spin-lock RF field frequencies were calibrated with a nutation experiment: after initial ^{1}H-^{15}N cross-polarization, a 5 ms spin-lock period was applied (to take into account possible detuning during a spin-lock, as this is relevant for a $R_{1\rho}$ experiment), followed by a 90 degree phase-shifted nutation pulse. If this pulse is a $\pi/2$ pulse, then the signal is zero. We determined the amplitude of this pulse by parametric incrementation. We find that two alternative calibration methods result in very similar calibrations: (i) a simple nutation pulse, applied at the beginning of the solvent-saturation period (see Figure S1), i.e. disregarding the spin-lock period, and (ii) the observation of the rotary resonance condition. For the latter, the signal intensity is monitored as a function of the ^{15}N spin-lock RF field strength in an experiment that applies a 5 ms spin-lock just after the initial ^{1}H-^{15}N CP transfer (Figure S1A); a minimum is observed when the RF field matches the n=1 rotary-resonance condition $\nu_{RF}= \nu_{MAS}$. We find that the three methods provide essentially identical calibration results. Processing and analysis was done with nmrPipe[16], and NMRView (OneMoon Scientific) as well as in-house written scripts in python language. Error estimates of rate constants were based on spectral noise estimates (3 times standard deviation of the signal in empty regions of the spectrum).

Numerical simulations

Simulations of the evolution of spin coherences were performed using in-house written programs using the GAMMA simulation library.[17] The simulation approach includes two spins (^{1}H , ^{15}N), existing in two exchanging sub-systems, spanning a composite Liouville space.[1,11,18,19] The simulation approach, as well as numerous results of similar kinds of simulations were reported recently.[1] Briefly, the evolution of the appropriate coherences (N_x, $2N_xH^{\alpha}$, $2N_xH^{\beta}$, H_z) is followed

over the course of a ^{15}N spin-lock. The two exchanging sub-states differ in the orientations of the ^{1}H-^{15}N dipolar coupling tensor and ^{15}N CSA tensor. The interaction tensor parameters were assumed as follows: ^{1}H-^{15}N dipolar coupling 22954 Hz (corresponding to 1.02 Å bond length), axially symmetric ^{15}N tensor with $\Delta\sigma$=-170 ppm, i.e. σ_{zz}=-113 ppm (6780 Hz at 14.1 T B_0 field strength). The ^{1}H CSA parameters have negligible effect in this context. The time-domain data were fitted with python scripts in order to obtain relaxation rate constants, using mono- or bi-exponential functions as reported in the text.

Results and Discussion

We first aim at providing a quantitative understanding of the effects of CSA/D CCR in $R_{1\rho}$ experiments by numerical simulations. Although a very well-established theoretical framework for nuclear spin relaxation exists (Redfield theory[20]), this theory is not strictly valid in cases of slow motion, which are the focus of this paper. Recent systematic analyses have established that Redfield results may disagree with numerical simulations,[1,7] even in cases where the actual relaxation is more than one order of magnitude slower than the dynamic event. In order to circumvent these problems we resort to numerical simulations for investigating the properties of $R_{1\rho}$ relaxation in rotating solids. The simulation approach is based on an explicit jump model of a ^{1}H-^{15}N moiety exchanging between two conformations. The employed composite Liouville-space approach has been used similarly before[11,18,19].

Figure 1 shows an example of a simulated decay of N_x coherence for a two-site exchange, using powder averaging and MAS. The observed decay (red curve in Figure 1A) is clearly non-exponential, and the exponential fit (black) unsatisfactorily describes the decay. The non-exponentiality may be ascribed to two effects. The first is that the NMR interactions that lead to relaxation (dipolar coupling, CSA) are orientation-dependent, and therefore the relaxation rate constants are orientation-dependent, too. When summing all contributions from different crystallite orientations across the sample, as required when considering a sample with randomly oriented crystallites, the resulting relaxation is always multi-exponential, as has been described and reviewed earlier.[1,21,22] If this is the only reason for non-monoexponential behavior, then individual crystallites (i.e. with a single orientation within the rotor-fixed frame) should show mono-exponential decays. However, we find that also when using single crystallites rather than a powder distribution the decay is bi-exponential (data not shown), pointing to an additional mechanism.

This second possible origin of non-exponential decay is the presence of cross-correlated relaxation due to ^{15}N-CSA/^{1}H-^{15}N dipolar-coupling interference. When observing the two components of the initial N_x coherence, namely the coherences N_x-[H^{α}] and N_x-[H^{β}], the decays are nearly exponential when integrated over a powder (Figure 1B). If one considers individual crystallites then the decay of the two coherences are indeed perfectly exponential (Figure S2C,D). One can readily show that the bi-exponential decay of N_x is due to interference of CSA and dipolar mechanisms: removing either of the two mechanisms (i.e. setting the jump angle for one of the two interactions to zero, or,

equivalently, setting the interaction strength to zero) leads to identical relaxation of the two components, and mono-exponential decay of N_x (data not shown). Furthermore, if a ^1H π pulse is inserted, thus inverting the sign of the dipolar interaction, the near-monoexponential decay is restored, as shown in Figure 1A (grey line). This is expected, as the effect of the cross-correlated relaxation is eliminated.

Numerical simulations also allow determining the difference of the rate constants of the two components, i.e. the CSA/D CCR rate constant in the $R_{1\rho}$ experiment, which we term here $\Gamma_{1\rho}^{CSA/D}$. Figure 2 establishes that the differential relaxation rate constant depends on the amplitude and time scale of the motion, as expected for a cross-correlated relaxation, and on the difference of RF field strength and MAS frequency, again as expected.[1,23] It exhibits a maximum when the motion is on the time scale of microseconds to tens of microseconds, in a manner that depends on the spin-lock RF field strength (Figure 2 E, F).

For completeness and illustration purposes, we also provide the analytical expression for the CCR rate constant under spin-lock, $\Gamma_{1\rho}^{CSA/D}$, in the framework of Redfield theory (which is only approximately valid[1]):

$$\Gamma_{1\rho}^{CSA/D} = \delta_{NH} \cdot \delta_{CSA} \cdot P_2(\cos(\theta)) \\ [\frac{3}{8} J(\omega_N) + \frac{1}{12} \cdot J(\omega_{RF} - 2\omega_{MAS}) + \frac{2}{12} \cdot J(\omega_{RF} - \omega_{MAS}) + \frac{1}{12} \cdot J(\omega_{RF} + 2\omega_{MAS}) + \frac{2}{12} \cdot J(\omega_{RF} + \omega_{MAS})] \quad (1)$$

Here, δ_{NH} is the anisotropy of the dipolar coupling tensor, δ_{CSA} is the chemical-shift anisotropy and $P_2(\cos(\theta))$ is the second Legendre polynomial involving the angle between the principal axes of the dipolar and CSA interactions, θ. It is interesting to confront this equation to the expression of the $R_{1\rho}$ relaxation rate constant due to the dipolar interaction and CSA, which is given as:[1,23]

$$R_{1\rho} = R_1 + \sin^2\theta_{eff} [R_{1\Delta} - \frac{1}{2} R_1] \quad \text{where}$$

$$R_{1\Delta} = \{\frac{\delta_{NH}}{4}\}^2 [3 \cdot J(\omega_N) + \frac{1}{3} \cdot J(\omega_{RF} - 2\omega_{MAS}) + \frac{2}{3} \cdot J(\omega_{RF} - \omega_{MAS}) + \frac{1}{3} \cdot J(\omega_{RF} + 2\omega_{MAS}) + \frac{2}{3} \cdot J(\omega_{RF} + \omega_{MAS})] \\ + \delta_{CSA}^2 [\frac{1}{3} \cdot J(\omega_{RF} - 2\omega_{MAS}) + \frac{2}{3} \cdot J(\omega_{RF} - \omega_{MAS}) + \frac{1}{3} \cdot J(\omega_{RF} + 2\omega_{MAS}) + \frac{2}{3} \cdot J(\omega_{RF} + \omega_{MAS})] \quad (2)$$

Comparison of (1) and (2) reveals that the two relaxation rate constants provide similar information. In this work we are interested primarily in motions slower than hundreds of nanoseconds (because in this range $\Gamma_{1\rho}^{CSA/D}$ and $R_{1\rho}$ are largest, as shown below); in this regime one can neglect the $J(\omega_N)$ term; furthermore, R_1 is very small compared to $R_{1\rho}$. Neglecting thus the $J(\omega_N)$ terms one can see that the two rate constants depend on the same spectral density functions (see Equations 1 and 2). We thus expect that the two rate constants are correlated, an observation that is indeed confirmed both experimentally and through simulations (discussed further below, Figures 2G and 3C). In the

remainder of this manuscript we do not use analytical calculations but use exclusively numerical simulations, because this allows to take into account additional factors, such as relaxation of the proton spin due to external mechanisms, as described below. By using numerical simulations we also circumvent the fact that Redfield theory is outside its range of validity for slow motions (microseconds).[1]

Experimental detection of CSA/D cross-correlated relaxation

In order to experimentally verify the effects of cross-correlated relaxation in $R_{1\rho}$ experiments, we prepared a sample of $^{2}H,^{15}N$ labelled microcrystalline ubiquitin. The protein was crystallized in a buffer that results in a re-protonation of exchangeable sites, such as the amide sites that we are interested in here, at a level of 60%. In such highly deuterated samples, narrow ^{1}H line widths can be achieved, and the simplicity of the spin system, that can be approximated as a two-spin system as far as ^{15}N relaxation is concerned, also allows for straightforward analysis of relaxation data.[24–26] Of particular relevance here, narrow ^{15}N lines are obtained even without ^{1}H decoupling, and therefore one can separately detect the decay of the doublet components. Figure 3 shows such ^{15}N $R_{1\rho}$ data for the ^{15}N doublet components of amide sites in ubiquitin, obtained at a MAS frequency of 38 kHz, and a ^{15}N RF field strength of 12 kHz. For the majority of residues the decay rate constants of the two components are detectably different. The differential relaxation rate constant of the two components, $\Gamma_{1\rho}^{CSA/D} = \{R_{1\rho}([N_xH^{\alpha}]) - R_{1\rho}([N_xH^{\beta}]\}/2$, varies across the protein sequence, ranging from close to zero to about 20 s^{-1} for different residues (Figure 3A). Residues located in secondary structure elements have small values, below 1 s^{-1} in most cases. Largest values of $\Gamma_{1\rho}^{CSA/D}$, exceeding 10 s^{-1}, are observed for residues G10 and K11 in the β1-β2 loop, which has been demonstrated before to undergo nanosecond motion in the microcrystals we are studying.[27,28] Cross-correlated relaxation rates are furthermore enhanced for residues located in the loop connecting β2 and ubiquitin's α-helix, the α-β3 loop and the loop connecting β4 to the short 3_{10} helix. These loop regions have also elevated $R_{1\rho}$ rate constants (Figure 3B). Figure 3C shows the correlation of residue-wise $\Gamma_{1\rho}^{CSA/D}$ and $R_{1\rho}$ rate constants. Because the majority of residues are located in secondary structure elements, residue-wise variations are generally small. Basically, only residues located in loop regions have significantly enhanced $\Gamma_{1\rho}^{CSA/D}$ and $R_{1\rho}$ rate constants. This limits the precision with which the correlation can be determined. The slope of the correlation is 1.48 when taking into account all residues (red line) and 1.96 when neglecting the two data points with largest rate constants. These experimental data unequivocally establish that the correlation has a non-zero offset: while $R_{1\rho}$ rate constants exceed 2 s^{-1} for all residues, many residues have a close-to-zero CSA/D cross-correlated relaxation rate constant. This finding cannot be understood based on the simulations in Figure 2. To understand this offset, one needs to take into account partial proton self-decoupling, as shown in the following section.

For completeness, we have also shown previously determined CSA/D CCR rate constants, determined with a spin-echo element instead of a spin-lock period. The drawback of the former

experiment is that the decay with free evolution (R_2') is significantly faster than decay under spin-lock (in ubiquitin by up to one order of magnitude). Consequently, it is more difficult to determine small CCR rates from the difference of the two comparably large decay rate constants corresponding to the two doublet components. Qualitatively, the three observables highlight the same residues undergoing slow motions.

It shall The correlation of the $\Gamma_{1\rho}^{CSA/D}$ rate constant

Proton spin diffusion and its effect on heteronuclear transverse relaxation

Longitudinal relaxation of the proton spin, or spin diffusion (i.e. magnetization exchange between protons) leads to interconversion of the spin states, α and β. Accordingly, the states $N_x[H^\alpha]$ and $N_x[H^\beta]$ inter-convert, and this would result in (partial) self-decoupling of these two ^{15}N doublet components. In the context of cross-correlated relaxation, such self-decoupling is an important parameter, because it is expected to reduce the CCR rate constant.[29] In this section we study the consequences of proton longitudinal relaxation or spin diffusion on heteronuclear relaxation and cross-correlated relaxation, using numerical simulations. At difference to the simulations shown in Figure 2, we added an *ad hoc* random field contribution acting on the proton spin. The effect of this random field is to relax the proton spin, and therefore interchange spin states H^α and H^β. In principle one might also attempt to explicitly simulate the proton spin diffusion or relaxation by using a large spin system with multiple protons. In practice, however, such simulations are prohibitively long if the spin system is larger than about 4-5 spins, and the accuracy of the proton evolution likely is not better than in our *ad hoc* external relaxation approach.

Figure 4 shows the results of numerical simulations of the heteronuclear $R_{1\rho}$ experiment in the presence of this additional proton relaxation, simulated here for the case of small-amplitude motion of the HN bond. Simulations with larger-amplitude motions are shown in Figure S3. These simulations establish that proton longitudinal relaxation induced by external relaxation mechanisms indeed reduces the CCR rate constant. The reduction of the $\Gamma_{1\rho}^{CSA/D}$ rate constant depends on the rate constant of the proton relaxation, as can be seen by comparison the red curves shown in panels (A) to (C). This reduction of $\Gamma_{1\rho}^{CSA/D}$ can be understood by the averaging of the two components. Figure 4 also shows that the ^1H spin flips have an effect on the $R_{1\rho}$ rate constants. For the range of $R_{1\rho}$ rate constants that are observed experimentally, i.e. in the range of $R_{1\rho}$ of a few s^{-1} to tens of s^{-1} at most, the proton relaxation leads to an increase in $R_{1\rho}$. The increase of $R_{1\rho}$ depends on the RF field strength and the MAS frequency (Figure S4). The origin of this increased $R_{1\rho}$ is the fact that stochastic proton spin flips counteract the MAS-induced recoupling of the dipolar interaction, as discussed in more detail in the Supporting Information. Taken together, the simulations of Figure 4 establish that the effect of the additional ^1H spin relaxation is (i) a reduction of the CCR rate constant, and (ii) an increase of the $R_{1\rho}$ rate constant. The decreased CCR and increased $R_{1\rho}$ rate constants change the slope of the correlation of the two rate constants, and result in an offset of the two rate constants (Figure 4D). It is remarkable that this situation is qualitatively found in the experimental data, shown in Figure 3C, which reproduce an offset of $R_{1\rho}$ rate constants. It shall be noted that Figure 4 assumes a single amplitude and varies the time scale of the motion, a situation

that is not likely to apply to the range of amide sites across a protein. Nonetheless, qualitatively the behavior observed in Figure 4 applies irrespectively of the precise motional model.

The amount by which the CCR rate is reduced depends on the rate at which the ^{1}H spin flip (Figure 4). We therefore need to estimate which spin diffusion rate constants are realistic in our experimental setting, i.e. at a MAS frequencies of 38 kHz and with the deuteration level we employed (60% back-exchange). Figure 5 shows experimental measurements of spin-diffusion between amide protons. By comparison of the spectra obtained with very short mixing time (100 μs, red) and 15 ms mixing (black), one can observe that there are additional peaks pointing to ^{1}H-^{1}H spin diffusion. Figure 5B highlights a few cases of well-resolved cross-peaks, corresponding to spin diffusion in a β-turn region (residues 45-47); for the cases of these cross-peaks, the corresponding amide sites are within ~4.2 Å at most. Figure 5C shows the time evolution of representative diagonal- and cross-peaks. The diagonal peaks show non-monoexponential decay, which we ascribe to contributions of spin-diffusion/cross-relaxation (fast component) and relaxation of the magnetization, presumably at the most dynamic sites, or through exchange with solvent. When fitting these curves with bi-exponential functions, respective rate constants are several tens per second for the fast rate (about 30-40% amplitude) and about 5-10 s^{-1} (60-70% amplitude), respectively. If attempting to describe the decay with a single rate constant, approximated by the time point where the signal decay to $1/e$ ~37%, apparent rate constants of 20 s^{-1} are obtained. The observable cross-peaks show a buildup within tens of milliseconds, similar to the fast rate observed in the diagonal-peak decay curves. Taken together, these data allow one to estimate that proton relaxation occurs at a rate of approximately 10-20 s^{-1}. (We note that the spin-diffusion rate is expected to decrease at higher MAS frequency and higher deuteration levels. A very recent report, which became available during the revision of the present manuscript,[30] used higher MAS frequencies (60 kHz), but lower deuteration (100% back-protonation of exchangeable sites), and values of about 10-20 s^{-1} were reported for the majority of the residues. While this is in rather good agreement with the present estimates, no apparent multi-exponential decay has been reported there, nor did the authors report on spin-diffusion cross-peaks.)

Using this estimate of ^{1}H relaxation, one can simulate its effect on measured $\Gamma_{1\rho}^{CSA/D}$ and $R_{1\rho}$ rate constants, and possibly correct for them. It has been proposed in solution-state NMR that ^{1}H-^{1}H NOE (i.e. relaxation-induced spin-diffusion) can be taken into account when analyzing cross-correlated relaxation,[31] using an analytical approach. In principle, such an approach could also be applied in solids. However, the effect of the proton spin flips on the ^{15}N relaxation depends on the RF field and the MAS frequency, and an appropriate formalism is currently not developed. However, one may resort to numerical simulations, such as the ones we use here, to evaluate the effects of proton spin flips on heteronuclear $R_{1\rho}$ or CCR rate constants. Experimentally determined proton decay rate constants, or at least global estimates, may be used to this end.

We illustrate this with the data shown in Figure 4. For example, assume that the experimentally determined $R_{1\rho}$ rate constant is 3 s^{-1}, i.e. including the effects of proton relaxation. The actual $R_{1\rho}$ rate constant, corrected for a ^{1}H relaxation rate constant of 20 s^{-1} (10 s^{-1}), is 1.8 s^{-1} (2.6 s^{-1}), i.e. the excess decay induced by the ^{1}H relaxation is of the order of 0.4 to 1.2 s^{-1}. In principle, one can take into account these effects, and use the corrected values when fitting motional models to transverse

relaxation data.

A similar estimation for $\Gamma_{1\rho}^{CSA/D}$ suggests, for example, that in the presence of a ^{1}H relaxation with a rate constant of 10 s^{-1}, a measured $\Gamma_{1\rho}^{CSA/D}$ of 1 s^{-1} points to an actual $\Gamma_{1\rho}^{CSA/D}$ rate constant of 3.6 s^{-1}. Arguably, it is more difficult to correct $\Gamma_{1\rho}^{CSA/D}$ for ^{1}H relaxation effects, because the values of this rate constant are smaller than those for $R_{1\rho}$, and ^{1}H relaxation has a stronger effect on $\Gamma_{1\rho}^{CSA/D}$ than on $R_{1\rho}$.

It is noteworthy that such a correction appears more difficult for the CCR rate constant, which may become very small and thus error-prone, than for $R_{1\rho}$. Of course, one may attempt to suppress the effects of proton spin flips even more, by using higher MAS frequencies and/or higher deuteration levels. Increasing MAS frequency will, however, not suppress proton magnetization decay which is actually due to dynamics or chemical exchange, such that it appears unlikely that one may suppress its effects completely.

Suppression of the effect of CSA/D CCR in $R_{1\rho}$ experiments

Finally, we note that the presence of CSA/D CCR might hamper accurate extraction of $R_{1\rho}$ rate constants. In solution-state NMR, schemes for suppression of the effect of CSA/D CCR have been reported.[13,32] They generally require irradiation of ^{1}H spins. Suppression of CCR in $R_{1\rho}$ experiments, even in solution-state NMR, is complicated by the fact that ^{1}H RF fields applied during heteronuclear spin-lock may partially re-introduce the scalar coupling Hamiltonian in solution and solids,[12,13] and it may also reintroduce the dipolar coupling in the solid state. In MAS ssNMR particular care has to be taken to avoid rotary resonance conditions, i.e. ^{1}H multi-pulse or CW schemes which counteract the averaging brought about by MAS. To investigate these effects, we have tested two different suppression schemes, namely (i) a single ^{1}H π pulse, applied in the center of the relaxation period and (ii) a train of ^{1}H π pulses, spaced by 5 ms delays. Both schemes, or variants thereof, are used in solution-state NMR.[12,13,33] Interestingly, we find that the multi-pulse scheme, even if the ^{1}H pulse spacing (5 ms) is very long compared to the rotor period (~20-30 μs), the heteronuclear coherences decay significantly faster than in the absence of ^{1}H pulses or with a single ^{1}H π pulse (Figure S5). The use of a single ^{1}H π pulse appears as a straightforward method to suppress the effects of CCR. We note, however, that even with a suppression of CCR, one does not expect mono-exponential decay, due to the inherent multi-exponential nature of decays in solids, outlined above.

Conclusions

We have shown here that CSA/D cross-correlated relaxation can be measured in MAS ssNMR of deuterated proteins. This relaxation rate constant reports on dynamics on nanosecond-to-microsecond time scales, as we illustrate with an application to microcrystalline ubiquitin. In many practical applications, however, the more easily accessible $R_{1\rho}$ rate constant of the decoupled line has advantages over the measurement of CSA/D CCR under spin-lock, in particular due to higher

sensitivity and resolution in a decoupled vs a non-decoupled spectrum. We also provided evidence, by numerical simulations, that rapid ^{1}H spin flips, as mediated by ^{1}H-^{1}H spin diffusion, reduces the CCR rate constant, and also contributes to the observed $R_{1\rho}$ rate constant. This finding also shows that for accurate quantitative analyses of $R_{1\rho}$ rate constants one should correct the measured rate constants for the contribution arising from proton relaxation. The present report of cross-correlated relaxation adds to the increasing arsenal of techniques to study protein dynamics on long time scales by MAS ssNMR, and stresses the importance of considering hitherto ignored effects when interpreting relaxation rate constants in ssNMR.

Supporting Information Description

Figures showing the pulse sequences used in this study; figures with additional simulations, and experimental data; extended discussion about the increase of $R_{1\rho}$ rate constants due to proton spin relaxation. This material is available free of charge via the Internet at http://pubs.acs.org.

Acknowledgements

This work was financially supported by the European Research Council (ERC-StG-311318 ProtDyn2Function) and the Commissariat a l'énergie atomique et aux énergies alternatives (CEA), the Centre National de la Recherche Scientifique (CNRS) and the Université Grenoble Alpes. This work used the platforms of the Grenoble Instruct Center (ISBG; UMS 3518 CNRS-CEA-UJF-EMBL) with support from FRISBI (ANR-10-INSB-05-02) and GRAL (ANR-10-LABX-49-01) within the Grenoble Partnership for Structural Biology (PSB). We thank Matthias Ernst for stimulating discussions and for assistance with implementing the proton random field fluctuations in the GAMMA simulations.

(1) Schanda, P.; Ernst, M. Studying Dynamics by Magic-Angle Spinning Solid-State NMR Spectroscopy: Principles and Applications to Biomolecules. *Prog. Nucl. Magn. Reson. Spectrosc.* **2016**, *96*, 1–46.

(2) Krushelnitsky, A.; Zinkevich, T.; Reichert, D.; Chevelkov, V.; Reif, B. Microsecond Time Scale Mobility in a Solid Protein as Studied by the 15N $R_{1\rho}$ Site-Specific NMR Relaxation Rates. *J. Am. Chem. Soc.* **2010**, *132*, 11850–11853.

(3) Lewandowski, J. R.; Sass, H. J.; Grzesiek, S.; Blackledge, M.; Emsley, L. Site-Specific Measurement of Slow Motions in Proteins. *J. Am. Chem. Soc.* **2011**, *133*, 16762–16765.

(4) Ma, P.; Haller, J. D.; Zajakala, J.; Macek, P.; Sivertsen, A. C.; Willbold, D.; Boisbouvier, J.; Schanda, P. Probing Transient Conformational States of Proteins by Solid-State R1rho Relaxation-Dispersion NMR Spectroscopy. *Angew. Chemie - Int. Ed.* **2014**, *53*, 4312–4317.

(5) Lamley, J. M.; Lougher, M. J.; Sass, H.-J.; Rogowski, M.; Grzesiek, S.; Lewandowski, J. R. Unraveling the Complexity of Protein Backbone Dynamics with Combined ^{13}C and ^{15}N Solid-state NMR Relaxation Measurements. *Phys. Chem. Chem. Phys.* **2015**, *17*, 21997–22008.

(6) Lamley, J. M.; Öster, C.; Stevens, R. A.; Lewandowski, J. R. Intermolecular Interactions and Protein Dynamics by Solid-State NMR Spectroscopy. *Angew. Chemie - Int. Ed.* **2015**, *54*, 15374–15378.

(7) Ma, P.; Xue, Y.; Coquelle, N.; Haller, J. D.; Yuwen, T.; Ayala, I.; Willbold, D.; Colletier, J.; Skrynnikov, N. R. Observing the Overall Rocking Motion of a Protein in a Crystal. *Nat Commun* **2015**, *6*, 1–24.

(8) Quinn, C. M.; McDermott, A. E. Quantifying Conformational Dynamics Using Solid-State $R_1\rho$ Experiments. *J. Magn. Reson.* **2012**, *222*, 1–7.

(9) Quinn, C. M.; McDermott, A. E. Monitoring Conformational Dynamics with Solid-State $R_1\rho$ Experiments. *J. Biomol. NMR* **2009**, *45*, 5–8.

(10) Chevelkov, V.; Diehl, A.; Reif, B. Quantitative Measurement of Differential 15-N-H A/β T2 Relaxation Rates in a Perdeuterated Protein by MAS Solid-State NMR Spectroscopy. *Magn. Reson. Chem.* **2007**, *45*, S156–S160.

(11) Skrynnikov, N. Asymmetric Doublets in MAS NMR: Coherent and Incoherent Mechanisms. *Magn. Reson. Chem.* **2007**, *45*, S161–S173.

(12) Massi, F.; Johnson, E.; Wang, C.; Rance, M.; Palmer, A. G. NMR $R_{1\rho}$ Rotating-Frame

Relaxation with Weak Radio Frequency Fields. *J. Am. Chem. Soc.* **2004**, *126*, 2247–2256.

(13) Korzhnev, D. M.; Skrynnikov, N. R.; Millet, O.; Torchia, D. A.; Kay, L. E. An NMR Experiment for the Accurate Measurement of Heteronuclear Spin-Lock Relaxation Rates. *J. Am. Chem. Soc.* **2002**, *124*, 10743–10753.

(14) Chevelkov, V.; Reif, B. TROSY Effects in MAS Solid-State NMR. *Concepts Magn. Reson. Part A* **2008**, *32A*, 143–156.

(15) Igumenova, T. I.; McDermott, A. E.; Zilm, K. W.; Martin, R. W.; Paulson, E. K.; Wand, a. J. Assignments of Carbon NMR Resonances for Microcrystalline Ubiquitin. *J. Am. Chem. Soc.* **2004**, *126*, 6720–6727.

(16) Delaglio, F.; Grzesiek, S.; Vuister, G.; Zhu, G.; Pfeifer, J.; Bax, A. NMRPIPE - a Multidimensional Spectral Processing System Based on Unix Pipes. *J. Biomol. NMR* **1995**, *6*, 277–293.

(17) Smith, S.; Levante, T.; Meier, B.; Ernst, R. Computer Simulations in Magnetic Resonance. An Object-Oriented Programming Approach. *J. Magn. Reson.*, **1994**, *106*, 75–105.

(18) Abergel, D.; Palmer, A. G. On the Use of the Stochastic Liouville Equation in Nuclear Magnetic Resonance: Application to $R_{1\rho}$ Relaxation in the Presence of Exchange. *Concepts Magn. Reson. Part A Bridg. Educ. Res.* **2003**, *19*, 134–148.

(19) Kubo, R. Stochastic Liouville Equations. *J. Math. Phys.* **1963**, *4*, 174–183.

(20) Redfield, A. G. On the Theory of Relaxation Processes. *IBM J. Res. Devel.* **1957**, *1*, 19–31.

(21) Torchia, D. A.; Szabo, A. Spin-Lattice Relaxation in Solids. *J. Magn. Reson.*, **1982**, *49*, 107–121.

(22) Giraud, N.; Blackledge, M.; Goldman, M.; Böckmann, A.; Lesage, A.; Penin, F.; Emsley, L. Quantitative Analysis of Backbone Dynamics in a Crystalline Protein from Nitrogen-15 Spin-Lattice Relaxation. *J. Am. Chem Soc.* **2005**, *127*, 18190–18201.

(23) Kurbanov, R.; Zinkevich, T.; Krushelnitsky, A. The Nuclear Magnetic Resonance Relaxation Data Analysis in Solids: General R1⁄R1ρ Equations and the Model-Free Approach. *J. Chem. Phys.* **2011**, *135*, 184104.

(24) Reif, B. Ultra-High Resolution in MAS Solid-State NMR of Perdeuterated Proteins: Implications for Structure and Dynamics. *J. Magn. Reson.* **2012**, *216*, 1–12.

(25) Schanda, P.; Huber, M.; Boisbouvier, J.; Meier, B. H.; Ernst, M. Solid-State NMR Measurements of Asymmetric Dipolar Couplings Provide Insight into Protein Side-Chain Motion. *Angew. Chem. Int. Ed. Engl.* **2011**, *50*, 11005–11009.

(26) Knight, M. J.; Webber, A. L.; Pell, A. J.; Guerry, P.; Barbet-Massin, E.; Bertini, I.; Felli, I. C.; Gonnelli, L.; Pierattelli, R.; Emsley, L.; et al. Fast Resonance Assignment and Fold Determination of Human Superoxide Dismutase by High-Resolution Proton-Detected Solid-State MAS NMR Spectroscopy. *Angew Chem Int. Ed. Engl.* **2011**, *50*, 11697–11701.

(27) Schanda, P.; Meier, B. H.; Ernst, M. Quantitative Analysis of Protein Backbone Dynamics in Microcrystalline Ubiquitin by Solid-State NMR Spectroscopy. *J. Am. Chem. Soc.* **2010**, *132*, 15957–15967.

(28) Haller, J. D.; Schanda, P. Amplitudes and Time Scales of Picosecond-to-Microsecond Motion in Proteins Studied by Solid-State NMR: A Critical Evaluation of Experimental Approaches and Application to Crystalline Ubiquitin. *J. Biomol. NMR* **2013**, *57*, 263–280.

(29) Hu, K.; Vögeli, B.; Clore, G. M. Interference between Transverse Cross-Correlated Relaxation and Longitudinal Relaxation Affects Apparent J-Coupling and Transverse Cross-Correlated Relaxation. *Chem. Phys. Lett.* **2006**, *423*, 123–125.

(30) Smith, A. A.; Testori, E.; Cadalbert, R.; Meier, B. H.; Ernst, M. Characterization of Fibril Dynamics on Three Timescales by Solid-State NMR. *J. Biomol. NMR* **2016**. DOI: 10.1007/s10858-016-0047-8

(31) Reif, B.; Diener, A.; Hennig, M.; Maurer, M.; Griesinger, C. Cross-Correlated Relaxation for the Measurement of Angles between Tensorial Interactions. *J. Magn. Reson.*, **2000**, *143*, 45–68.

(32) Massi, F.; Johnson, E.; Wang, C.; Rance, M.; Palmer, A. G. NMR R1rho Rotating-Frame Relaxation with Weak Radio Frequency Fields. *J. Am. Chem. Soc.* **2004**, *126*, 2247–2256.

(33) Palmer, A. G.; Massi, F. Characterization of the Dynamics of Biomacromolecules Using Rotating-Frame Spin Relaxation NMR Spectroscopy. *Chem. Rev.* **2006**, *106*, 1700–1719.

(34) Clore, G. M.; Driscoll, P. C.; Wingfield, P. T.; Gronenborn, A. M. Analysis of the Backbone Dynamics of Interleukin-1 Beta Using Two-Dimensional Inverse Detected Heteronuclear ^{15}N-^{1}H NMR Spectroscopy. *Biochemistry* **1990**, *29*, 7387–7401.

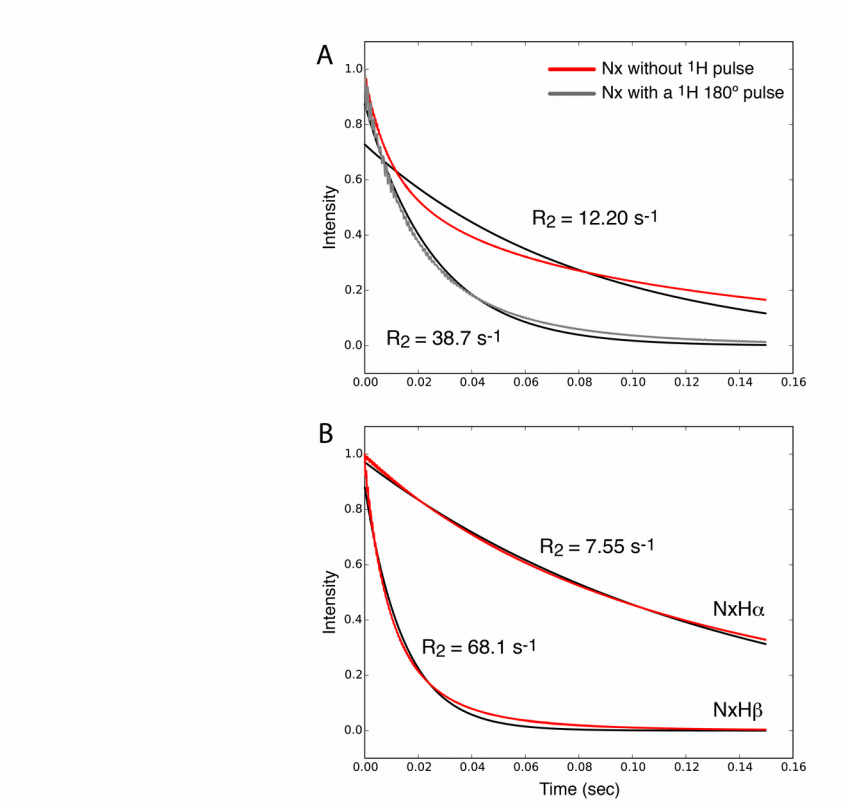

Figure 1: Simulated evolution of ^{15}N spin coherences under a spin-lock RF field. (A) Time evolution of in-phase N_x coherence (red) and a single-exponential fit, which clearly results in poor agreement with the decay. For the simulation shown in grey, a ^{1}H π pulse was inserted in the center of the spin-lock period. An exponential fit is shown in black. (B) Simulation of the doublet components, N_x-[H^{α}], N_x-[H^{β}] (red), and exponential fits (black). The jump angle was 20 degrees and the jump rate constant 30000 s^{-1}.

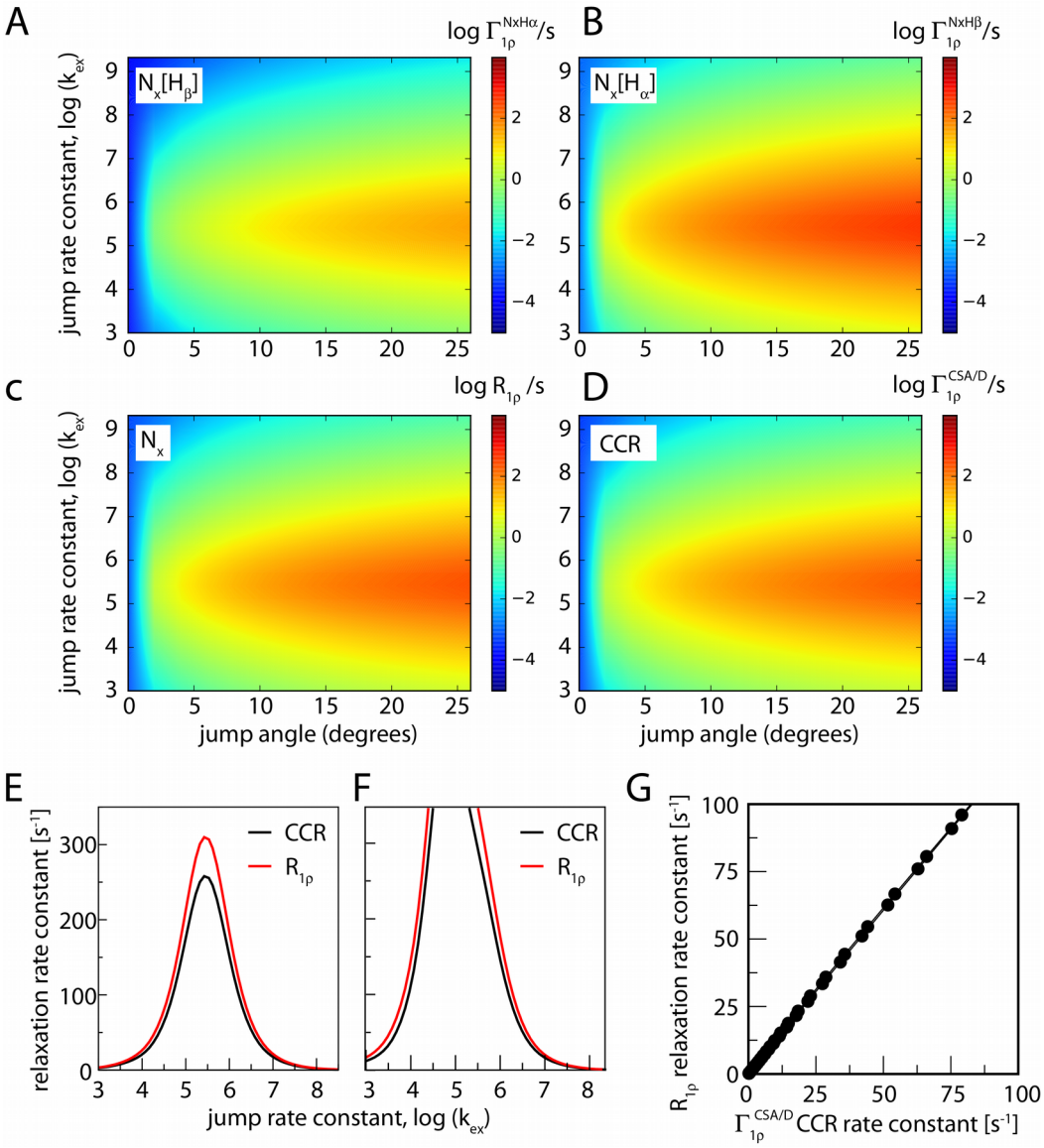

Figure 2:

Simulated relaxation rate constants of a ^{15}N spin due to its CSA tensor and ^{1}H-^{15}N dipolar coupling, within the two-site jump model. Shown are rate constants for the individual doublet components (A, B), the average rate constant $R_{1\rho}$ (C) and the CSA/D CCR rate constant (D), as a function of the jump angle and jump rate constant. (E) shows $R_{1\rho}$ and CCR rate constants for a constant jump angle (20º) as a function of the jump rate constant, assuming a MAS frequency of 40 kHz and a RF field strength of 12 kHz. (F) uses parameters as in (E), but with an RF field strength of 32 kHz. (G) Correlation of $R_{1\rho}$ and CCR rate constants, assuming a jump angle of 5º and a MAS frequency of 40 kHz and a RF field strength of 12 kHz. The jump angle can be related to the often-used order parameter S^2 as $S^2=1/4\left(3\cos^2(\theta)+1\right)$.[34] According to this equation, jump angles of 5, 10, 15, 20, 25 degrees, for example, correspond to S^2= 0.994, 0.977, 0.95, 0.91, 0.866, respectively.

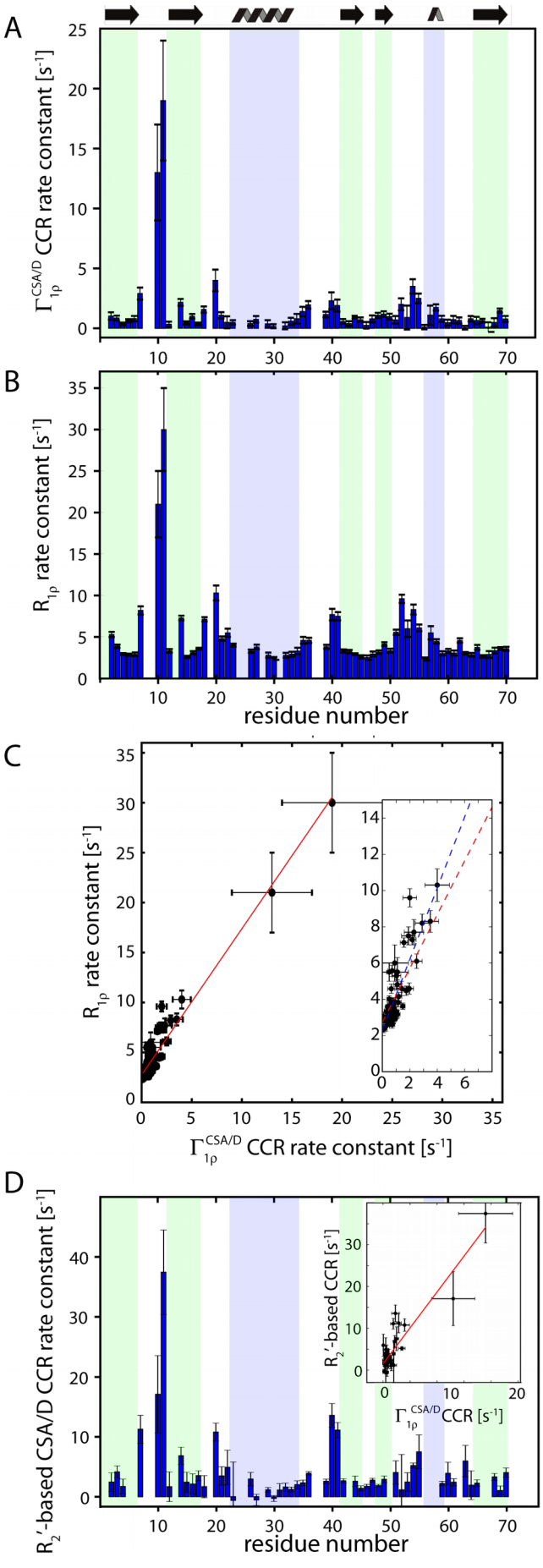
A
B
C
D
residue number
$\Gamma_{1\rho}^{CSA/D}$ CCR rate constant [s^{-1}]
$R_{1\rho}$ rate constant [s^{-1}]
R_2'-based CSA/D CCR rate constant [s^{-1}]
R_2'-based CCR [s^{-1}]
$\Gamma_{1\rho}^{CSA/D}$CCR [s^{-1}]

Figure 3: Experimental observation of CSA/D CCR in ^{15}N spin-lock relaxation experiments in deuterated, 60% back-exchanged ubiquitin, obtained at a MAS frequency of 38 kHz. (A) Differential relaxation rate constants as a function of the residue number, determined from the relaxation rate constant of the two doublet components. (B) $R_{1\rho}$ relaxation rate, i.e. obtained from the average of the two rate constants. In (C), a correlation of the two rate constants is shown. The red line corresponds to a correlation obtained over all available residues, with a slope of 1.48 and an intercept of 2.74 s^{-1}. The insert focuses on the data points at low rate constants. The blue line has a slope of 1.96 s^{-1}. Panel (D) shows previously published[27] CSA/D CCR relaxation rate constants, obtained with a spin-echo (delay – π pulse – delay) sequence instead of a spin-lock, at the same B_0 field strength. The insert shows the correlation of these data with the $R_{1\rho}$-based CCR rate constants of panel (A).

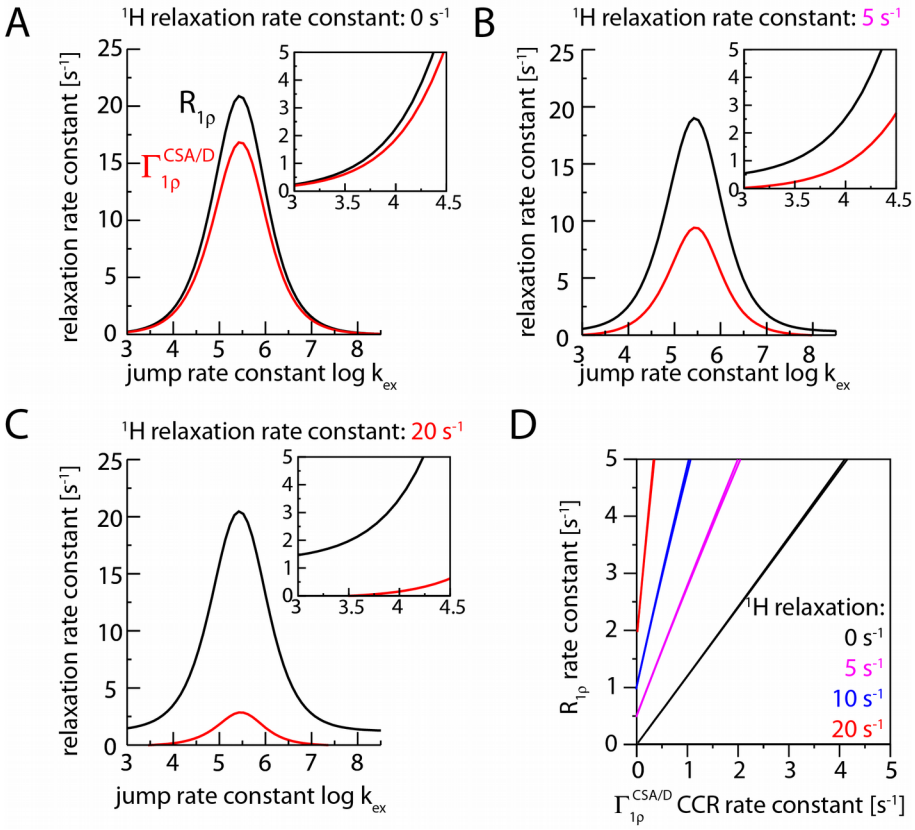

Figure 4: The effect of proton relaxation on ^{15}N transverse relaxation parameters, from numerical simulations with an *ad hoc* added random field fluctuation leading to proton relaxation. Shown are the simulated relaxation rate constants of N_x (i.e. the relaxation with a ^1H π pulse in the center of the spin-lock relaxation period), $R_{1\rho}$, and the cross-correlated relaxation rate constant, $\Gamma_{1\rho}^{CSA/D}$, obtained from the differences of relaxation of the two doublet components. Different rate constants of the ^1H relaxation are assumed: 0 s^{-1} (A), 5 s^{-1} (B) and 20 s^{-1} (C); $R_{1\rho}$ and $\Gamma_{1\rho}^{CSA/D}$ rate constants are shown in black and red, respectively. Panel (D) correlates the $R_{1\rho}$ and $\Gamma_{1\rho}^{CSA/D}$ relaxation rate constants for different ^1H relaxation rate constants. The jump angle was set to 5 degrees, corresponding to an order parameter of S^2=0.994. More simulations with a large motional amplitude are shown in Figure S3.

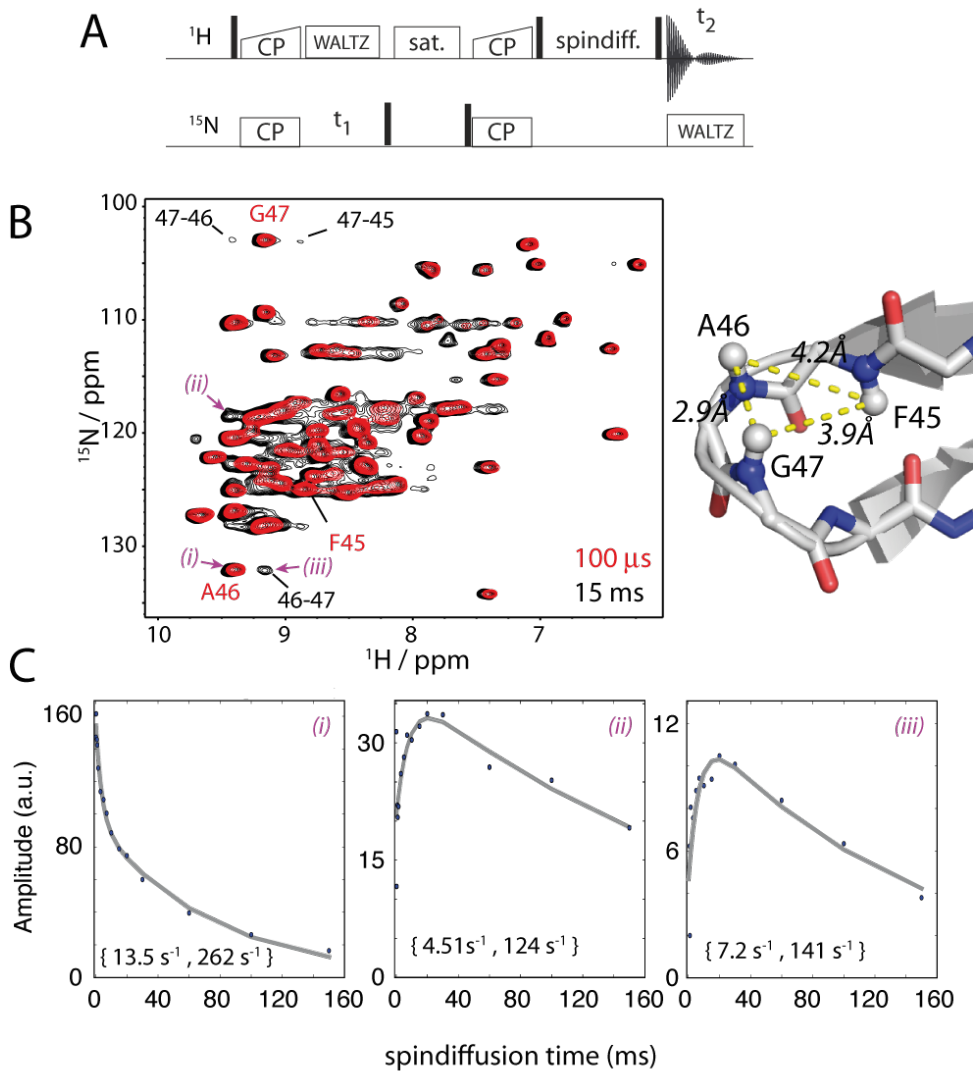

Figure 5: Experimental investigation of proton relaxation and spin diffusion in the deuterated, 60% back-exchanged ubiquitin sample at 38 kHz MAS (14.1 T). (A) Pulse sequence used to detect ^{1}H relaxation/spin diffusion. (B) Overlay of two spectra obtained with different mixing times as indicated. Selected amide peaks, and the corresponding spin-diffusion cross-peaks are indicated, and the distances between these sites are indicated on the right. (C) Representative time traces observed at peak positions corresponding to amide sites (diagonal peaks), and two spin-diffusion cross-peaks, obtained at spectral positions at which intensity is observed only with a mixing time. The grey lines correspond to bi-exponential fits, and the fitted rate constants are indicated in brackets. The identity of the peaks for which the graphs are shown in C is indicated in the spectrum with *(i)-(iii)*.

TOC Figure